INTERNATIONAL JOURNAL FOR NUMERICAL METHODS IN FLUIDS, VOL. 23, 787–809 (1996)

SPLIT, CHARACTERISTIC BASED SEMI-IMPLICIT ALGORITHM FOR LAMINAR/TURBULENT INCOMPRESSIBLE FLOWS

O. C. ZIENKIEWICZ, B. V. K. SATYA SAI, K. MORGAN AND R. CODINA

Institute for Numerical Methods in Engineering, University of Wales, Swansea SA2 8PP, U.K.

SUMMARY

In an earlier paper, Zienkiewicz and Codina (*Int. j. numer. methods fluids*, **20**, 869–885 (1995)) presented a general algorithm for the solution of both compressible and incompressible Navier–Stokes equations. The algorithm, based on operator splitting, permits arbitrary interpolation functions to be used while avoiding the Babŭska–Brezzi restriction. In addition, its characteristic based approach introduces a form of rational dissipation. Zienkiewicz *et al. (Int. j. numer. methods fluids*, **20**, 887–913 (1995)) presented the application of this algorithm in its fully explicit form to various inviscid compressible flow problems. They also presented two incompressible flow problems solved by the fully explicit form, employing a pseudo compressibility. The present work deals with the application of the above algorithm it its semi-implicit form to some incompressible flow benchmark problems. Further, it extends the methodology to turbulent flows by employing both one, and two equation turbulence models. A comparison of results with earlier investigations is presented. Other issues addressed in this study include the effect of additional diffusion terms present in the scheme for both laminar and turbulent flow problems and some practical difficulties associated with local time stepping.

KEY WORDS: operator-splitting; general algorithm; characteristic-Galerkin; laminar/turbulent; incompressible

1. INTRODUCTION

The development of Galerkin finite element procedures for the incompressible Navier–Stokes equations can be dated back to the 1970s, when Hood and Taylor[1] advocated the use of mixed interpolation with interpolation functions for pressure being at least one order less than those used for velocities. Equal-order interpolation gives rise to spurious pressure modes as a result of zero diagonal terms in the discrete steady state equations which prove singular, thus violating the Babŭska–Brezzi (B–B) restriction. Penalty forms avoid this difficulty by introducing a small non-zero term in the diagonal, but they are not robust and are doomed to fail unless the B–B condition is satisfied *a priori*, as is the case with certain kinds of reduced integration.[2] Thus alternative stabilization methods are desirable. Hughes *et al.*[3] have shown that such stabilization could be achieved by the addition of terms corresponding to those arising from the application of a least squares method. Sani *et al.*[4,5] provided some more suggestions to deal with checkerboard pressure modes and on the use of a penalty formulation without reduced integration for the penalty term. However, the same stabilization could be achieved in a natural way in many time-stepping formulations when the steady state solution is reached. The fractional step method, devised originally by Chorin[6] in a finite difference context,

CCC 0271–2091/96/080787–23

Received January 1996
Revised January 1996

forms the basis for many of the finite element formulations[7–10] that employ operator splitting. The method essentially separates the pressure calculation into one involving a Laplacian form which is self-adjoint. This method, when applied to obtain the steady state solution, can in certain forms circumvent the B–B restriction, as observed by Schneider *et al.*[7] and Kawahara and Ohmiya[8] and clearly explained by Zienkiewicz and Wu.[11]

The treatment of convection-dominated flows poses another difficulty in the simulation of incompressible flows. The application of the conventional Galerkin finite element method to a scalar convection dominated problem is equivalent to central differencing of the convection terms, which causes 'wiggles' or complete instabilities to appear in the flow variables. Thus the traditional Galerkin finite element method is no longer optimal when convection phenomena dominate the flow. A possible way of dealing with wiggles is to refine the mesh in convection dominated regions.[12] A more economical approach is to use upwind differences or, more generally, a suitable Petrov–Galerkin method, which not only suppresses the oscillations but also improves the accuracy of computation. Originally proposed by Christie *et al.*,[13] the upwind finite element method was later pursued and improved upon by Heinrich *et al.*,[14] Hughes and Brookes,[15] Kelly *et al.*[16] and Johnson *et al.*[17]

Another, more rational, way to obtain the upwinding effect in scalar problems is to use a characteristic based time-marching scheme,[18] which provides an effective time-stepping procedure for transient solutions as well as an iterative procedure for steady state solutions. This concept forms the basis for the development of a general algorithm based on operator-splitting to deal with both the compressible and incompressible Navier–Stokes equations.[19]

In the present work this general algorithm in its semi-implicit form is used and extended to deal with turbulent incompressible flows. It is also intended in the present work to bring out the effect of additional dissipation terms (which contribute to the upwinding effect) present in the characteristic-based formulation. A general observation by earlier investigators is that while oscillation free results could be obtained with upwinding for laminar flow problems, for turbulent predictions, upwinding could lead to an underprediction of such quantities as turbulent kinetic energy and reattachment lengths.[20] We find that this assertion is not generally true and that the present algorithm yields good results also in the turbulent regime. The problems dealt with in the present work to address the above issues include laminar flow over a backward facing step, laminar flow in a lid-driven cavity and turbulent flow over a backward facing step.

A rigorous mathematical derivation of the algorithm is presented in Reference 19. Here we present the extension of this scheme to turbulence modelling using both one and two equation models of turbulence.

2. EQUATIONS OF FLOW

The governing equations for a Newtonian, incompressible viscous flow are written as

$$\nabla \cdot \mathbf{u} = 0 \quad \text{(continuity)}, \tag{1}$$

$$\frac{\partial \mathbf{u}}{\partial t} = \nabla \cdot [-(\mathbf{u} \otimes \mathbf{u}) - P\mathbf{I} + \boldsymbol{\tau} + \mathbf{f}^e] \quad \text{in} \quad \Omega \times (0, T) \quad \text{where } \Omega \subset \mathbb{R}^2 \quad \text{(momentum)}, \tag{2}$$

where $\mathbf{u}$ is the vector of velocities (U_1, U_2), P is the pressure divided by the density (p/ρ), $\boldsymbol{I}$ is the unit tensor, $\boldsymbol{\tau}$ is the shear stress tensor divided by the density, $\mathbf{f}_e$ is the body force vector.

The shear stress tensor (divided by the density) $\boldsymbol{\tau}$ is given by

$$\tau_{ij} = \nu\left(\frac{\partial U_i}{\partial x_j} + \frac{\partial U_j}{\partial x_i} - \tfrac{2}{3}\nabla \cdot \mathbf{u}\delta_{ij}\right), \quad i,j = 1, 2. \tag{3}$$

Of course, the third term within the brackets on the right-hand side of this equation becomes equal to zero by virtue of equation (1).

For turbulent flows the Reynolds-averaged Navier–Stokes equations are derived by assuming that any flow variable ϕ can be written as

$$\phi = \bar{\phi} + \phi', \tag{4}$$

where $\bar{\phi}$ is the mean turbulent value and ϕ' is the fluctuating component. Then the Reynolds-averaged Navier–Stokes equations become

$$\nabla \cdot \bar{\mathbf{u}} = 0 \quad \text{(continuity)}, \tag{5}$$

$$\frac{\partial \bar{\mathbf{u}}}{\partial t} = \nabla \cdot [-(\bar{\mathbf{u}} \otimes \bar{\mathbf{u}}) - \bar{P}\mathbf{I} + \boldsymbol{\tau}^{\mathrm{V}} + \boldsymbol{\tau}^{\mathrm{R}} + \mathbf{f}_{\mathrm{e}}] \quad \text{(momentum)}. \tag{6}$$

Here $\boldsymbol{\tau}^{\mathrm{V}}$ is the viscous shear stress tensor divided by the density, as defined by equation (3), and $\boldsymbol{\tau}^{\mathrm{R}}$ is the Reynolds shear stress tensor divided by the density, defined as

$$\boldsymbol{\tau}^{\mathrm{R}} = -\overline{\mathbf{u}' \otimes \mathbf{u}'} \tag{7}$$

or, in Cartesian co-ordinates,

$$\tau_{ij}^{\mathrm{R}} = -\overline{U_i' U_j'}. \tag{8}$$

In the present study, first order closure models have been employed. In this kind of modelling the Boussinesq's assumption is used, which relates the turbulent shear stresses to a turbulent eddy viscosity which in turn is calculated by means of either a one or a two equation model. Employing the Boussinesq's assumption, we write

$$\tau_{ij}^{\mathrm{R}} = -\overline{U_i' U_j'} = \nu_{\mathrm{T}} \left(\frac{\partial \bar{U}_i}{\partial x_j} + \frac{\partial \bar{U}_j}{\partial x_i} - \tfrac{2}{3} \nabla \cdot \bar{\mathbf{u}} \delta_{ij} \right) - \tfrac{2}{3} \kappa \delta_{ij}. \tag{9}$$

Here ν_{T} is the turbulent eddy kinematic viscosity coefficient and κ is the turbulent kinetic energy given by $\frac{1}{2}\overline{(\mathbf{u}')^2}$. The momentum equation becomes

$$\frac{\partial \bar{\mathbf{u}}}{\partial t} = \nabla \cdot [-(\bar{\mathbf{u}} \otimes \bar{\mathbf{u}}) - \bar{P}\mathbf{I} + \boldsymbol{\tau}^{\mathrm{T}} + \mathbf{f}_{\mathrm{e}}], \tag{10}$$

where

$$\boldsymbol{\tau}^{\mathrm{T}} = \boldsymbol{\tau}^{\mathrm{V}} + \boldsymbol{\tau}^{\mathrm{R}} = (\nu + \nu_{\mathrm{T}}) \left(\frac{\partial \bar{U}_i}{\partial x_j} + \frac{\partial \bar{U}_j}{\partial x_i} - \tfrac{2}{3} \nabla \cdot \bar{\mathbf{u}} \delta_{ij} \right) - \tfrac{2}{3} \kappa \delta_{ij}. \tag{11}$$

To close the system of equations, the Prandtl–Kolmogorov relationship

$$\nu_{\mathrm{T}} = c_{\mu}' \kappa^{1/2} L \tag{12}$$

is used, where $\kappa^{1/2}$ is a velocity scale for large scale turbulent motion (indeed, κ is the turbulent kinetic energy), L is a length scale for turbulence and c_{μ}' is a constant. In the present study both one and two equation models have been used, which differ in the way in which equation (12) is evaluated.

2.1. One equation model

An additional transport equation is solved for κ, the turbulent kinetic energy, while a simple algebraic relation is used for L, the length scale. The equation for κ is of the form

$$\frac{\partial \kappa}{\partial t} = -\nabla \cdot (\kappa \bar{\mathbf{u}}) + \nabla \cdot (\nu_\kappa \nabla \kappa) + (\boldsymbol{\tau}^R \cdot \nabla) \cdot \bar{\mathbf{u}} - \epsilon. \tag{13}$$

The first term on the right hand side is the convective component, the second term is the diffusion component, the third term is the turbulence production term and the fourth term is the dissipation term. Also,

$$\nu_\kappa = \nu + \frac{\nu_T}{\sigma_\kappa}, \tag{14}$$

where σ_κ is a constant taken generally as unity. Further,

$$\epsilon = C_D \frac{\kappa^{3/2}}{L}, \tag{15}$$

where C_D is a constant. The turbulence length scale L and the mixing length, l_m are related by the expression[21]

$$l_m = \left(\frac{(c'_\mu)^3}{C_D} \right)^{1/4} L. \tag{16}$$

Various possibilities are available for evaluating the mixing length l_m.[21] In the present work the Prandtl mixing length has been used, in which $l_m = 0{\cdot}4y$, where y is the distance to the nearest wall. Combining equations (12) and (16), ν_T is given as

$$\nu_T = (c'_\mu C_D)^{1/4} \kappa^{1/2} l_m \quad \text{or} \quad \nu_T = c_\mu^{1/4} \kappa^{1/2} l_m, \tag{17}$$

where c_μ is a constant taken generally as 0·09.

2.2. Two equation model

Here the transport equation

$$\frac{\partial \epsilon}{\partial t} = -\nabla \cdot (\epsilon \bar{\mathbf{u}}) + \nabla \cdot (\nu_\epsilon \nabla \epsilon) + C_{\epsilon 1} \frac{\epsilon}{\kappa} (\boldsymbol{\tau}^R \cdot \nabla) \cdot \bar{\mathbf{u}} - C_{\epsilon 2} \frac{\epsilon^2}{\kappa} \tag{18}$$

is used to evaluate ϵ where $C_{\epsilon 1}$ is a constant taken in the range 1·45–1·55 and $C_{\epsilon 2}$ is a constant in the range 1·92–2·00. Also,

$$\nu_\epsilon = \nu + \frac{\nu_T}{\sigma_\epsilon}, \tag{19}$$

where σ_ϵ is a constant taken equal to 1·3.

In two equation models, ν_T is evaluated by the formula

$$\nu_T = c_\mu \frac{\kappa^2}{\epsilon}. \tag{20}$$

Frequently the initial and boundary conditions for the above models are taken in the form κ and ϵ given at $t = 0$,

$$\kappa|_\Gamma = 0, \qquad \epsilon|_\Gamma = \epsilon_b,$$

where Γ is a solid boundary. However, in general, ϵ_b is not known. Further, these models are not valid near walls where the local *Re* is too small. To account for the near-wall effects, either wall functions or low Reynolds number versions have to be used. In the present analysis, low Reynolds number versions have been employed for both one and two equation models. This simply involves a modification of various coefficients of the original models by multiplying them by suitable damping functions.

2.3. *Low Re version of the one equation model*

Wolfstein[22] suggested the modifications

$$\nu_t = c_\mu^{1/4} \kappa^{1/2} l_m f_\mu, \tag{21}$$

$$\epsilon = C_D \frac{\kappa^{3/2}}{L f_b}, \tag{22}$$

where

$$f_\mu = 1 - e^{-0{\cdot}160 R_k}, \qquad f_b = 1 - e^{-0{\cdot}263 R_k}, \qquad R_k = \sqrt{\kappa}\frac{y}{\nu}$$

and y is the distance from the nearest wall.

2.4. *Low Re version of the two equation model*

According to Lam and Bermhorst,[23] the coefficients c_μ, $C_{\epsilon 1}$ and $C_{\epsilon 2}$ appearing in the two equation model are multiplied by damping functions f_μ, $f_{\epsilon 1}$ and $f_{\epsilon 2}$ respectively. Here

$$f_\mu = (1 - e^{-0{\cdot}0165 R_k})^2 \left(1 + \frac{20{\cdot}5}{R_t}\right), \tag{23}$$

$$f_{\epsilon 1} = 1 + \left(\frac{0{\cdot}05}{f_\mu}\right)^3, \tag{24}$$

$$f_{\epsilon 2} = 1 - e^{-R_t^2}, \tag{25}$$

where $R_t = \kappa^2/\nu\epsilon$. The wall boundary conditions are now $\kappa = 0$ and $\partial\epsilon/\partial y = 0$.

3. SOLUTION METHODOLOGY

Reverting to the notation used in Reference 19 and dropping the overbar for turbulent averaged quantities for convenience, the full system of equations can be represented as

$$\frac{\partial V}{\partial t} + \frac{\partial F_i}{\partial x_i} + \frac{\partial G_i}{\partial x_i} + Q = 0, \tag{26}$$

where

$$V^T = [0, U_1, U_2, \kappa, \epsilon] \tag{27}$$

is the independent variable vector (note that ϵ does not appear for the one-equation model),

$$F_i^T = \left[U_i, U_1 U_i + \delta_{1i}\left(P + \tfrac{2}{3}\kappa\right), U_2 U_i + \delta_{2i}\left(P + \tfrac{2}{3}\kappa\right), U_i\kappa, U_i\epsilon\right] \tag{28}$$

is the convective flux vector,

$$G_i^{\mathrm{T}} = \left[0, -\tau_{1i}^{\mathrm{T}}, -\tau_{2i}^{\mathrm{T}}, -\left(\nu + \frac{\nu_{\mathrm{T}}}{\sigma_\kappa}\right)\frac{\partial \kappa}{\partial x_i}, -\left(\nu + \frac{\nu_{\mathrm{T}}}{\sigma_\epsilon}\right)\frac{\partial \epsilon}{\partial x_i}\right] \tag{29}$$

is the viscous flux vector and

$$Q^{\mathrm{T}} = \left[0, g_1, g_2, -\tau_{ij}^{\mathrm{R}}\frac{\partial U_i}{\partial x_j} + \epsilon, -C_{\epsilon 1}\frac{\epsilon}{\kappa}\tau_{ij}^{\mathrm{R}}\frac{\partial U_i}{\partial x_j} + C_{\epsilon 2}\frac{\epsilon^2}{\kappa}\right]. \tag{30}$$

The various steps involved in the discretization of such equations have been explained in Reference 19. Here we only present a summary of the steps and the extension to the incompressible κ and ϵ equations. In all the ensuing equations the standard Galerkin procedure is used with the discretization

$$\begin{aligned} U_i &= N\bar{U}_i, & \Delta U_i &= N\Delta\bar{U}_i, & \Delta\tilde{U}_i &= N\Delta\tilde{\bar{U}}_i, & P &= N_{\mathrm{p}}\bar{P}, \\ \kappa &= N\bar{\kappa}, & \epsilon &= N\bar{\epsilon}, & \Delta\kappa &= N\Delta\bar{\kappa}, & \Delta\epsilon &= N\Delta\bar{\epsilon}, \end{aligned} \tag{31}$$

where an overbar denotes the finite element nodal values.

Step 1

Evaluate an intermediate auxiliary variable $\tilde{\bar{U}}$ for $\bar{U}$ such that

$$\Delta\tilde{\bar{U}} = -\mathbf{M}^{-1}\Delta t[(\mathbf{C}\bar{U} + \mathbf{K}\bar{U} - \mathbf{f}) - \Delta t(\mathbf{K}_{\mathrm{u}}\bar{U} + \mathbf{f}_{\mathrm{s}})]^n. \tag{32}$$

The matrices in the above equation are evaluated as

$$\begin{aligned} \mathbf{M} &= \int_\Omega N^{\mathrm{T}}N\,\mathrm{d}\Omega, & \mathbf{C} &= \int_\Omega N\frac{\partial(\bar{U}_i N^{\mathrm{T}})}{\partial x_i}\,\mathrm{d}\Omega, \\ \mathbf{K} &= \int_\Omega (\nu + \nu_{\mathrm{T}})\frac{\partial N^{\mathrm{T}}}{\partial x_i}\frac{\partial N}{\partial x_i}\,\mathrm{d}\Omega + \text{boundary terms}, & \mathbf{f} &= \int_\Omega N^{\mathrm{T}}\frac{2}{3}\frac{\partial(N\bar{\kappa})}{\partial x_i}\,\mathrm{d}\Omega, \\ \mathbf{K}_{\mathrm{u}} &= \frac{1}{2}\int_\Omega \frac{\partial}{\partial x_i}(\bar{U}_i N^{\mathrm{T}})\frac{\partial}{\partial x_j}(\bar{U}_j N)\,\mathrm{d}\Omega, & \mathbf{f}_{\mathrm{s}} &= -\frac{1}{2}\int_\Omega \frac{\partial}{\partial x_i}(\bar{U}_i N^{\mathrm{T}})\frac{2}{3}\frac{\partial(N\bar{\kappa})}{\partial x_i}\,\mathrm{d}\Omega. \end{aligned} \tag{33}$$

Step 2

Solve a Poisson equation for pressure,

$$\Delta t^2\theta_1\theta_2\mathbf{H}\Delta\bar{P} = \Delta t[\mathbf{Q}(\bar{U} + \theta_1\Delta\tilde{\bar{U}}) - \Delta t\theta_1\mathbf{H}\bar{P} - \mathbf{f}_{\mathrm{p}}]^n, \tag{34}$$

where

$$\mathbf{H} = \int_\Omega \frac{\partial N_{\mathrm{p}}^{\mathrm{T}}}{\partial x_i}\frac{\partial N_{\mathrm{p}}}{\partial x_i}\,\mathrm{d}\Omega, \qquad \mathbf{Q} = \int_\Omega \frac{\partial N_{\mathrm{p}}^{\mathrm{T}}}{\partial x_i}N\,\mathrm{d}\Omega. \tag{35}$$

Step 3

Correct the velocity via

$$\Delta\bar{U} = \Delta\tilde{\bar{U}} - \mathbf{M}^{-1}\Delta t[\mathbf{Q}^{\mathrm{T}}(\bar{P} + \theta_2\Delta\bar{P}) + \Delta t\mathbf{P}\bar{P}]^n, \tag{36}$$

$$\mathbf{P} = \frac{1}{2}(1-\theta_2)\int_\Omega \frac{\partial}{\partial x_2}(\bar{U}_i N_{\mathrm{p}}^{\mathrm{T}})\frac{\partial N_{\mathrm{p}}}{\partial x_i}\,\mathrm{d}\Omega, \tag{37}$$

where θ_1 and θ_2 are integration parameters and $\theta_1, \theta_2 \in [0, 1]$.

Step 4

Using $\bar{U}$ and $\bar{P}$, evaluate κ in the one equation model or both κ and ϵ in the two equation model as

$$\Delta\bar{\kappa} = -\Delta t[\mathbf{C}\bar{\kappa} + \mathbf{K}_\kappa\bar{\kappa} + \mathbf{f}_\kappa - \Delta t(\mathbf{K}_{\mathrm{u}}\bar{\kappa} + \mathbf{f}_{\kappa\mathrm{s}})]^n, \tag{38}$$

where

$$\begin{aligned}
\mathbf{K}_\kappa &= \int_\Omega \frac{\partial N^{\mathrm{T}}}{\partial x_i}\left(\nu + \frac{\nu^{\mathrm{T}}}{\sigma_\kappa}\right)\frac{\partial N}{\partial x_i}\,\mathrm{d}\Omega + \text{boundary terms.}\\
\mathbf{f}_\kappa &= \int_\Omega N^{\mathrm{T}}\left[\left(\tau_{ij}^{\mathrm{R}}\frac{\partial\bar{U}_i}{\partial x_j}\right) - \bar{\epsilon}\right]\mathrm{d}\Omega, \qquad \mathbf{f}_{\kappa\mathrm{s}} = -\frac{1}{2}\int_\Omega \frac{\partial}{\partial x_i}(\bar{U}_i N^{\mathrm{T}})\tau_{ij}^{\mathrm{R}}\frac{\partial\bar{U}_i}{\partial x_j}\,\mathrm{d}\Omega,
\end{aligned} \tag{39}$$

and

$$\Delta\bar{\epsilon} = -\Delta t[\mathbf{C}\bar{\epsilon} + \mathbf{K}_\epsilon\bar{\epsilon} + \mathbf{f}_\epsilon - \Delta t(\mathbf{K}_{\mathrm{u}}\bar{\epsilon} + \mathbf{f}_{\epsilon\mathrm{s}})]^n, \tag{40}$$

where

$$\begin{aligned}
\mathbf{K}_\epsilon &= \int_\Omega \frac{\partial N^{\mathrm{T}}}{\partial x_i}\left(\nu + \frac{\nu^{\mathrm{T}}}{\sigma_\epsilon}\right)\frac{\partial N}{\partial x_i}\,\mathrm{d}\Omega + \text{boundary terms,}\\
\mathbf{f}_\epsilon &= \int_\Omega N^{\mathrm{T}}\left[\left(C_{\epsilon 1}\frac{\bar{\epsilon}}{\bar{\kappa}}\tau_{ij}^{\mathrm{R}}\frac{\partial\bar{U}_i}{\partial x_j}\right) - C_{\epsilon 2}\frac{\bar{\epsilon}^2}{\bar{\kappa}}\right]\mathrm{d}\Omega,\\
\mathbf{f}_{\epsilon\mathrm{s}} &= -\frac{1}{2}\int_\Omega \frac{\partial}{\partial x_i}(\bar{U}_i N^{\mathrm{T}})\left(C_{\epsilon 1}\frac{\bar{\epsilon}}{\bar{\kappa}}\tau_{ij}^{\mathrm{R}}\frac{\partial\bar{U}_i}{\partial x_j} - C_{\epsilon 2}\frac{\bar{\epsilon}^2}{\bar{\kappa}}\right)\mathrm{d}\Omega.
\end{aligned} \tag{41}$$

It should be noted that the treatment of the turbulent quantities brings an additional term f and its associated second-order term $\mathbf{f}_{\mathrm{s}}$ into (32). These terms are defined in (33). Thus an additional upwinding effect is produced by the presence of $\mathbf{f}_{\mathrm{s}}$.

The treatment of boundary conditions in the finite element approximation is discussed in Reference 19 and in more detail in Reference 24. In the latter reference it is shown that the conventionally used procedure of imposing U_i on $\bar{U}_i$ on solid boundaries is incorrect and a more rational procedure avoids this. In all the examples presented here, the procedure outlined in Reference 24 has been used.

4. CHOICE OF TIME STEP

Equation (32) above is conditionally stable. Applying a linear stability analysis to the one dimensional convection–diffusion equation, the critical time step can be shown to be

$$\Delta t_{\text{crit}} = \frac{h}{|u|}\left[\sqrt{\left(\frac{1}{Pe^2}+1\right)}-\frac{1}{Pe}\right], \tag{42}$$

where h is a representative element length, $|u|$ is the maximum velocity in the element and Pe is the Peclet number, defined as

$$Pe = |u|h/\nu. \tag{43}$$

If the time-stepping scheme is operated locally at or near the critical stability limit, the steady state solution reached will be close to that resulting from the optimal Petrov–Galerkin process for the steady state.[2] This requires that the critical time step be evaluated at each node and be used for time stepping at that node. However, on some occasions this could give rise to unrealistic differences in local time steps at different nodes in the flow domain, which could in turn result in the collapse of the computation. For example, in the wall-driven cavity problem which is presented later, near the top wall the mesh size is small and the associated velocities are large so as to give a very small time step. In contrast, at the centre of the cavity the mesh size is large and the associated velocities are small so as to give a very large time step. Another option is to choose a locally optimal value for the 'interior Δt' (that occurring inside the square brackets in equations (32), (34), (36), (38) and (40)) and use a globally minimum value for the 'exterior Δt'. A preliminary study on the cavity problem for various Reynolds numbers has been conducted using this methodology. However, the velocity field was observed to be damped by an excessive additional diffusion. Thus for further studies in this paper a globally minimum value of the time step was used for both internal and external Δt. The critical time step, as evaluated by equations (42) and (43), is applicable for laminar flow problems only, where the diffusion terms are only those arising owing to the viscous shear stresses. For turbulent flow problems, to account for the Reynolds stresses, the simple modification

$$Pe = |u|h/(\nu + \nu_{\text{T}}) \tag{44}$$

is made to equation (43). In the case of the two equation model for turbulence, the ϵ equation poses severe restrictions on the time step owing to the presence of the troublesome source term. Thus the overall time step has to be less than that predicted by equation (42). The strategies used in the present study to overcome this restriction are discussed in the next section.

5. SOURCE TERM IN THE TWO EQUATION MODEL

While the critical time step for laminar viscous flows is given by equation (42), for the κ–ϵ model the time step is further restricted by the source term $C_{\epsilon 2}\epsilon^2/\kappa$. In the limit $t \to 0$ the κ–ϵ model is extremely 'stiff' near the wall boundaries, since $\kappa = 0$ on the walls. As a result, the two-equation model requires more time steps to reach convergence than the one-equation model. One way of removing this problem is to specify initial profiles for κ and ϵ to guarantee convergence. This is not always possible in complex flow situations. There are two possible ways of avoiding this difficulty.

1. Neglect the source term in the ϵ equation until such time that the solution develops and reasonable profiles for κ and ϵ develop near the walls.
2. Use a fixed mixing length for the initial development ('warm-up') of the solution. This means using equation (15) for ϵ in equation (13). After a few thousand time steps the fixed mixing

length can be turned off and ϵ can be used in equation (13). This is the method that has been used in the present work when employing the two equation model.

6. NUMERICAL CALCULATIONS

The following benchmark problems have been chosen to evaluate the performance of the present scheme for incompressible flows:

(a) laminar flow over a backward facing step
(b) laminar flow in a lid-driven cavity
(c) turbulent flow over a backward facing step.

For all three cases both the present scheme and the standard velocity correction scheme (standard Galerkin plus operator splitting) have been run for comparison. It may be remarked here that the standard velocity correction (SVC) scheme could be recovered from the present scheme by simply

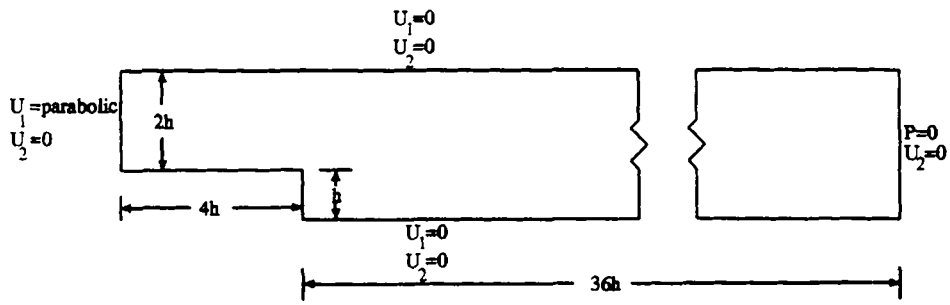

Figure 1(a). Geometry and boundary conditions for laminar flow past a backward facing step

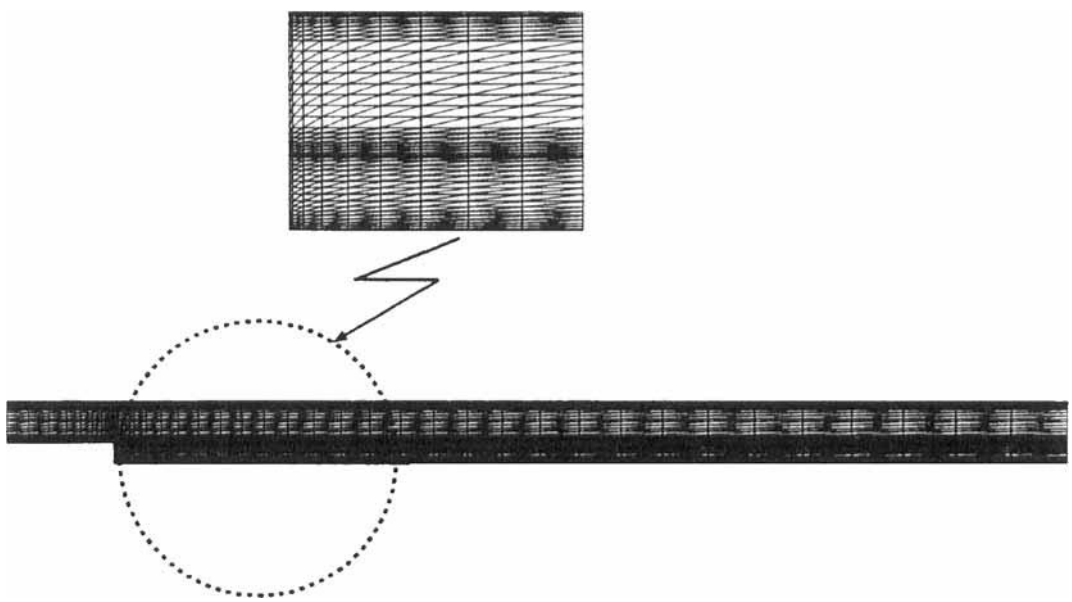

Figure 1(b). Mesh (1537 nodes, 2912 elements) for laminar flow past a backward facing step

dropping the second-order terms (which contribute to the upwinding effect). The first two examples demonstrate the accuracy of the present scheme. Further, in the first example the present scheme gives a better prediction of reattachment lengths as compared with the SVC. Also, for both these examples the pressure field predictions are smoother than with the SVC. The third example illustrates the application of the present scheme to turbulence modelling using both the one- and two-equation models of turbulence. For all the problems, non-uniform structured meshes with linear triangular elements have been useed. A banded Gaussian solver has been used to solve the pressure Poisson equation (34).

6.1. Laminar flow over a backward facing step

Experimental results for this case are provided by Denham and Patrick.[25] The cases considered are $Re = 73$, 191 and 229. The Reynolds number is based on the average velocity at the entrance and the height of the step. The expansion ratio of the step is 2 : 3. The entry is at a distance of 4 step heights upstream of the step. The outflow boundary has been taken sufficiently far away (36 step heights downstream of the step) to obtain undisturbed flow conditions at the outlet. Figure 1(a) shows the geometry and boundary conditions and Figure 1(b) shows the finite element mesh for the problem. The mesh with 1537 nodes and 2912 elements is non-uniformly spaced, with fine meshes near the wall. Figures 2(a)–2(c) show the pressure contours with the present scheme (top) and the SVC (bottom) for $Re = 73$, 191 and 229 respectively. The present scheme yields smoother pressure fields than the SVC. Further, for $Re = 191$ and 229, for the mesh employed, the SVC fails to yield a meaningful result, as can be seen from Figure 2(c). For $Re = 191$ the U_1-velocity profiles at various sections behind the step have been plotted in Figure 3. The experimental results of Denham and Patrick[25] and the SVC results have also been plotted for comparison. There is close agreement between the present scheme and the SVC except in the vicinity of the reattachment point. Also, good agreement with the experimental results[25] can be observed. The most common criterion to judge the performance of various numerical schemes for this problem is the prediction of the reattachment length behind the step. In Figure 4 a comparison of the reattachment lengths predicted by the present scheme, the SVC and Taylor *et al.*[26] and the experimental results[25] is presented. This shows that the present scheme yields better results than the scheme of Taylor *et al.*,[26] who used an upwinding proposed by Heinrich *et al.*[14] Note that the reattachment length prediction by the SVC for $Re = 229$ is not shown in the figure, as the solution could not be obtained for this. Table I gives the reattachment length predictions by the various methods and the percentage errors from the experimental results of Denham and Patrick.[26]

In general, the predictions by the present scheme appear to be better than those of Taylor *et al.*[26] and the SVC. Finally, Figure 5 shows the streamline contours by the present scheme for the three Reynolds numbers mentioned above. The enlarged views near the step are also shown for each case.

Table I. Comparison of reattachment lengths by various methods (figures in brackets indicate percentage errors from experimental results of Denham and Patrick[25])

Re	Denham and Patrick[25]	Taylor *et al.*[26]	S–G method	Present
73	3·9	5·3 (35·9)	4·9 (25·6)	4·8 (23·0)
191	8·6	9·4 (9·3)	9·7 (12·7)	9·2 (7·0)
229	10·0	11·4 (14·0)	—	10·9 (9·0)

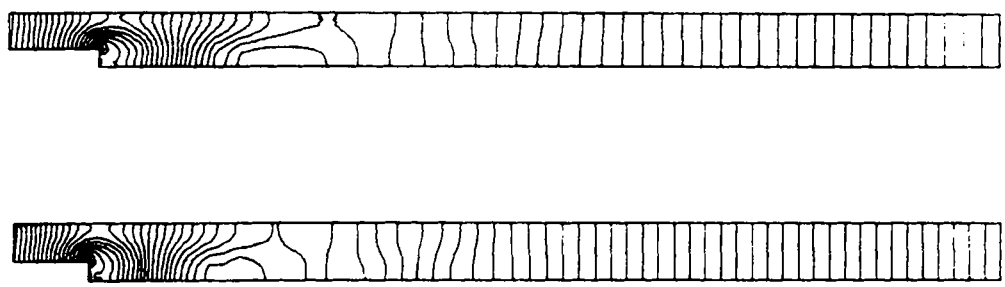

(a) Re = 73

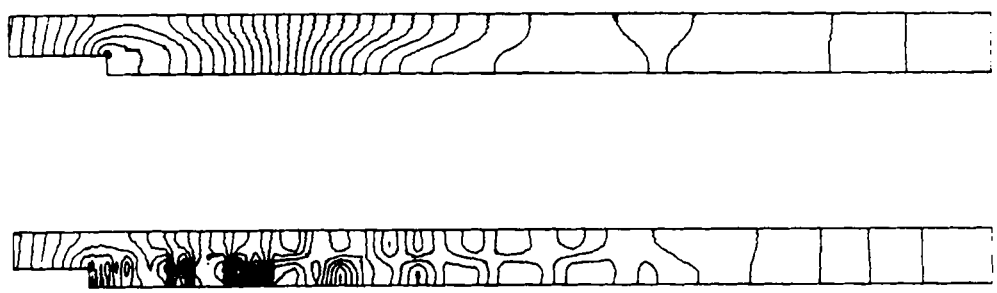

(b) Re = 191

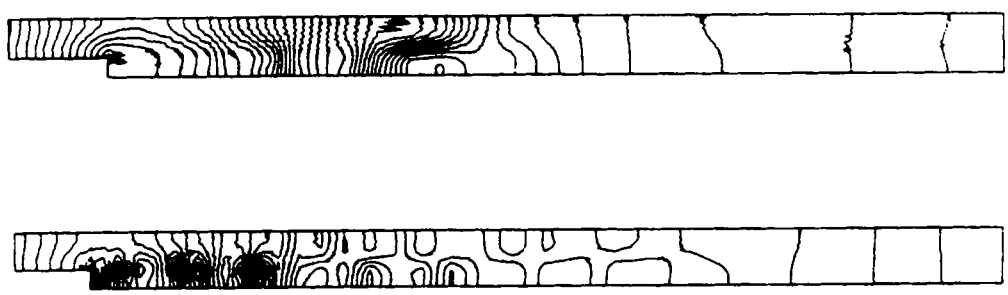

(c) Re = 229

Figure 2. Pressure contours for laminar flow past a backward-facing step: top, present scheme (upwind); bottom, SVC (no upwind)

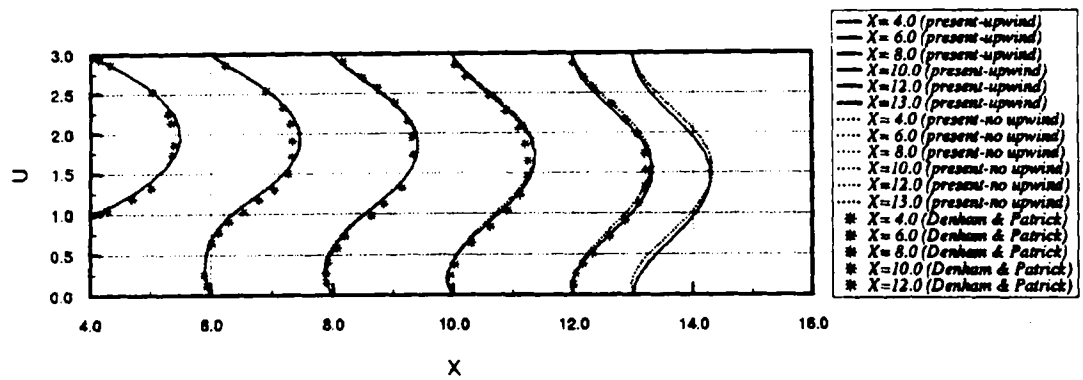

Figure 3. Velocity profiles downstream of step for $Re = 191$

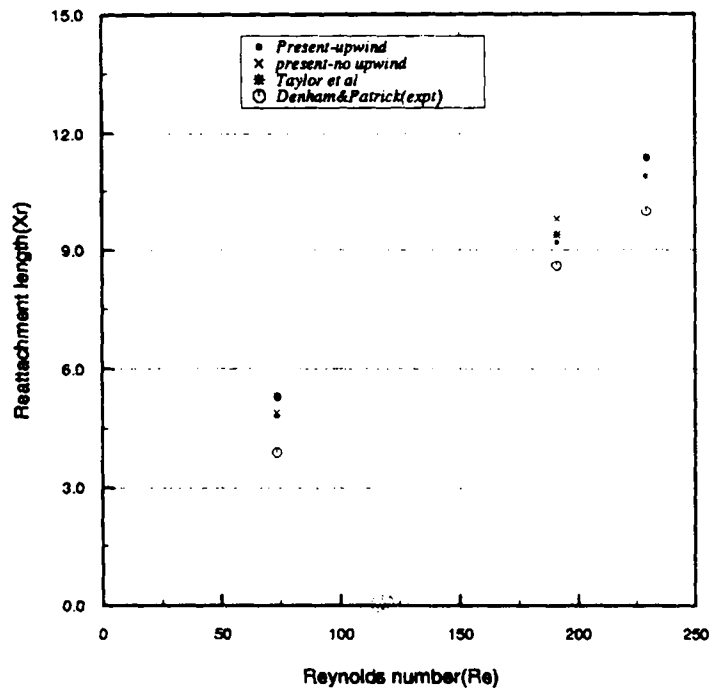

Figure 4. Comparison of reattachment lengths with various schemes

6.2. Laminar flow in a lid-driven cavity

Figure 6(a) shows the geometry and boundary conditions for this problem. A zero-velocity condition exists on all the walls except the top one, which moves with a (non-dimensional) horizontal velocity equal to unity. The non-dimensional pressure at the middle point of the bottom wall is fixed as zero. Figure 6(b) shows the mesh for this problem, which consists of 1521 nodes and 2888 elements. Based on some preliminary studies with two different meshes, it was observed that this mesh is sufficiently fine for the present study. The Reynolds numbers investigated are 400, 1000 and

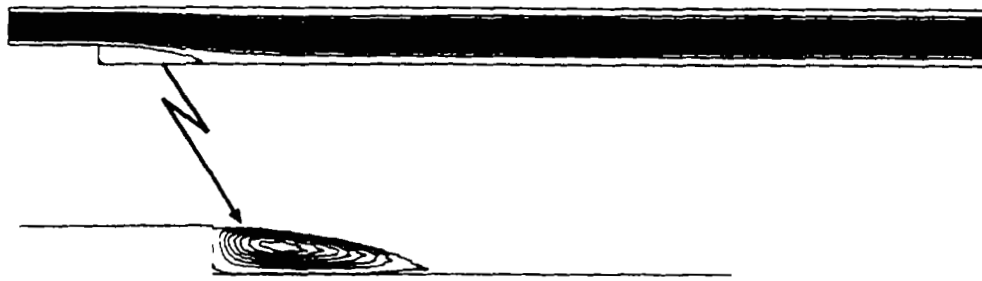

(a) Re = 73

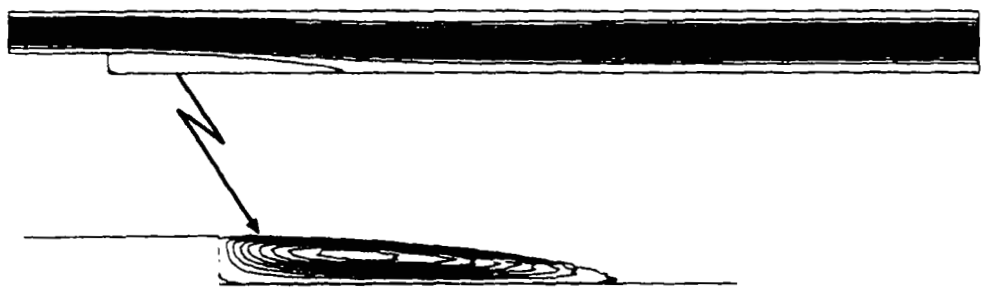

(b) Re = 191

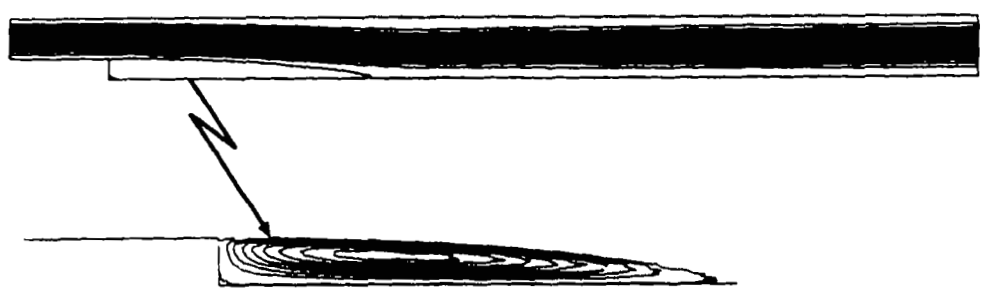

Figure 5. Streamline patterns for various Reynolds numbers with present scheme

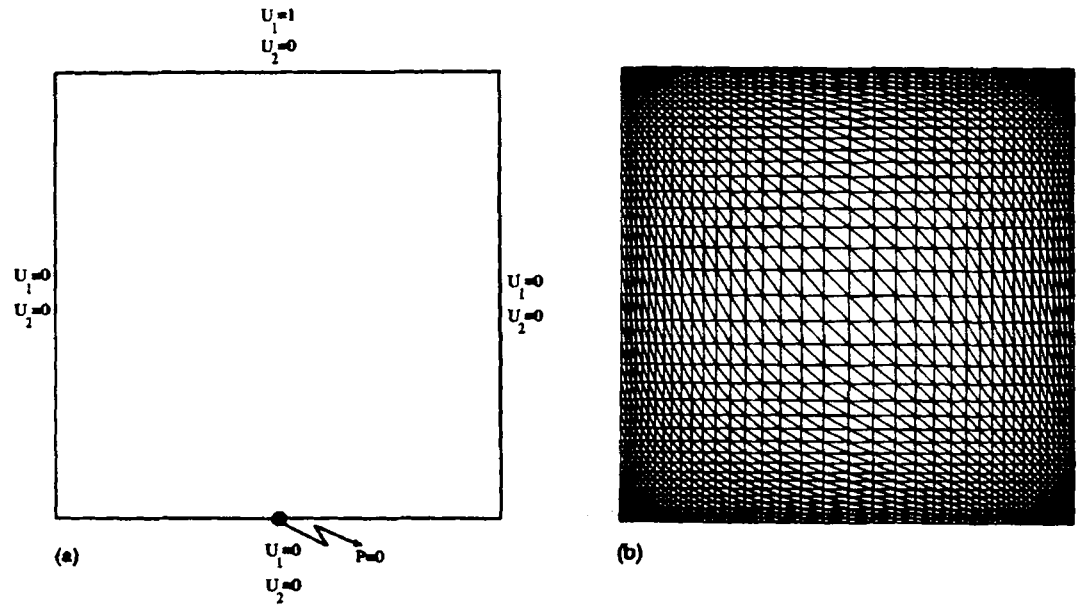

Figure 6. Laminar flow in a lid-driven cavity: (a) geometry and boundary conditions; (b) mesh (1521 nodes, 2888 elements)

5000. Once again, both the present scheme and the standard velocity correction (SVC) method have been run on this mesh. Figures 7(a)–7(c) show the pressure contours for the two schemes for $Re = 400$, 1000 and 5000 respectively. The left sequence shows the pressure contours with the present scheme, while the right sequence shows the same with the SVC. As expected, the pressure contours with the present scheme, especially at higher Re, are smoother and more wiggle-free than those with the SVC. Figure 8(a) shows the U_1-velocity profile along the mid-vertical plane for $Re = 400$ with both schemes. Also plotted are the benchmark values obtained by Ghia *et al.*[27] using a multigrid strategy with the streamfunction–vorticity formulation. From this figure it can be noticed that the present scheme and the SVC give more or less the same result. A very small amount of damping could be observed with the present scheme which can be attributed to the presence of additional diffusion terms. A somewhat different observation has been made by Sohn,[28] who used a BTD-type upwinding for the same problem. In his case the upwinding resulted in a substantial amount of damping. Figures 8(b) and 8(c) show similar comparisons for $Re = 1000$ and 5000 respectively. Figures 9(a)–9(c) show the streamline patterns and Figures 10(a)–10(c) show the velocity vectors for $Re = 400$, 1000 and 5000 respectively with the present scheme.

The above two examples demonstrate the application of the present scheme in its semi-implicit form for laminar incompressible flow problems. While giving accurate solutions to both problems, the present scheme has also been able to provide smoother pressure fields as compared with the SVC.

6.3. Turbulent flow over a backward facing step

This problem is widely chosen to test the numerical performance of turbulence codes. Both one and two equation models have been used by Atkins *et al.*[20] and Taylor *et al.*[26] and the two equation model has been used by Sohn,[28] Hackman *et al.*[29] and Autret *et al.*,[30] while experimental results are provided by Denham *et al.*[31] The geometry used for this problem is similar to the one for the laminar flow problem, but the outlet is considered at 24 step heights downstream of the step. The Reynolds

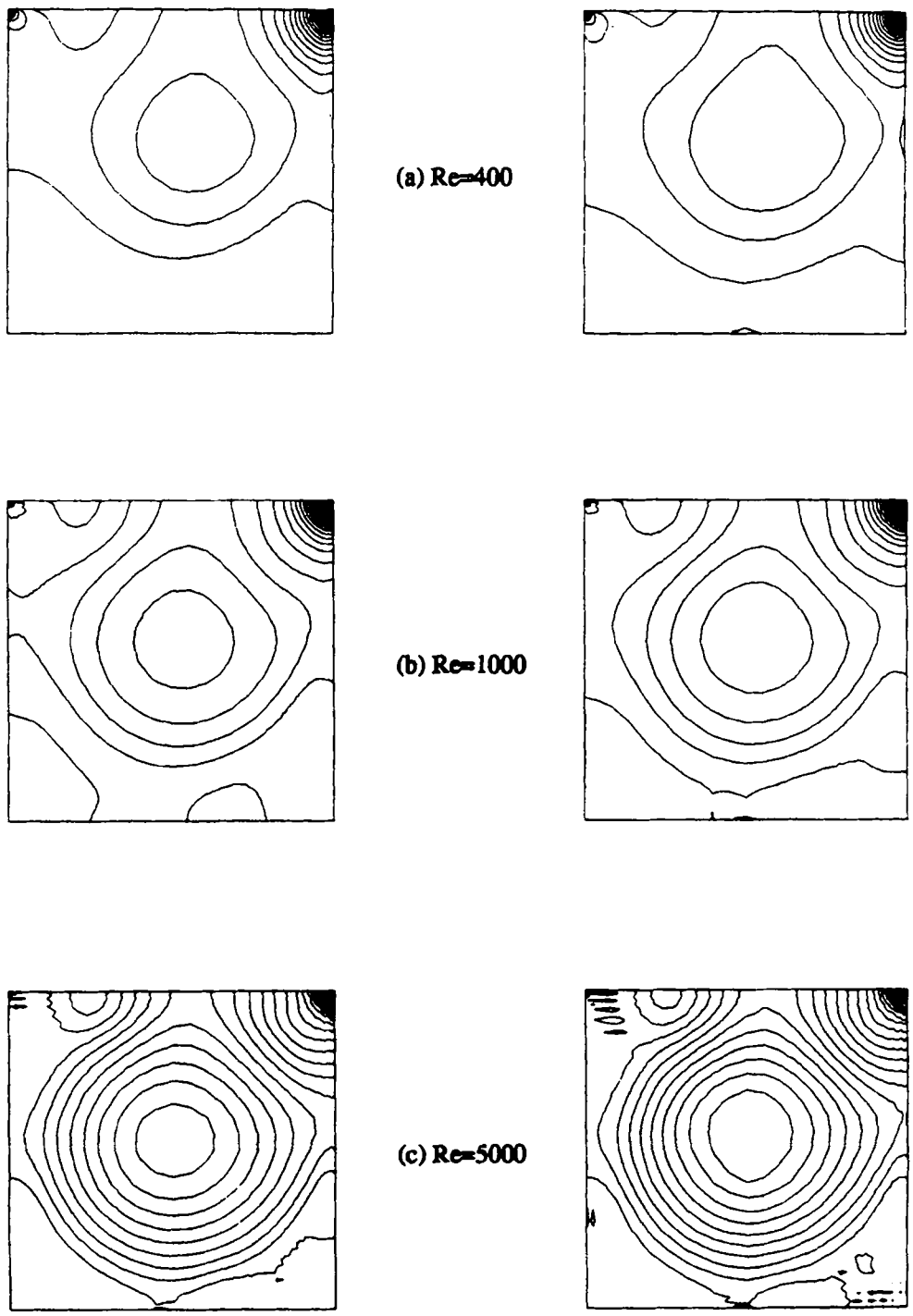

Figure 7. Pressure contours for various Reynolds numbers: left, present scheme (upwind); right, SVC (no upwind)

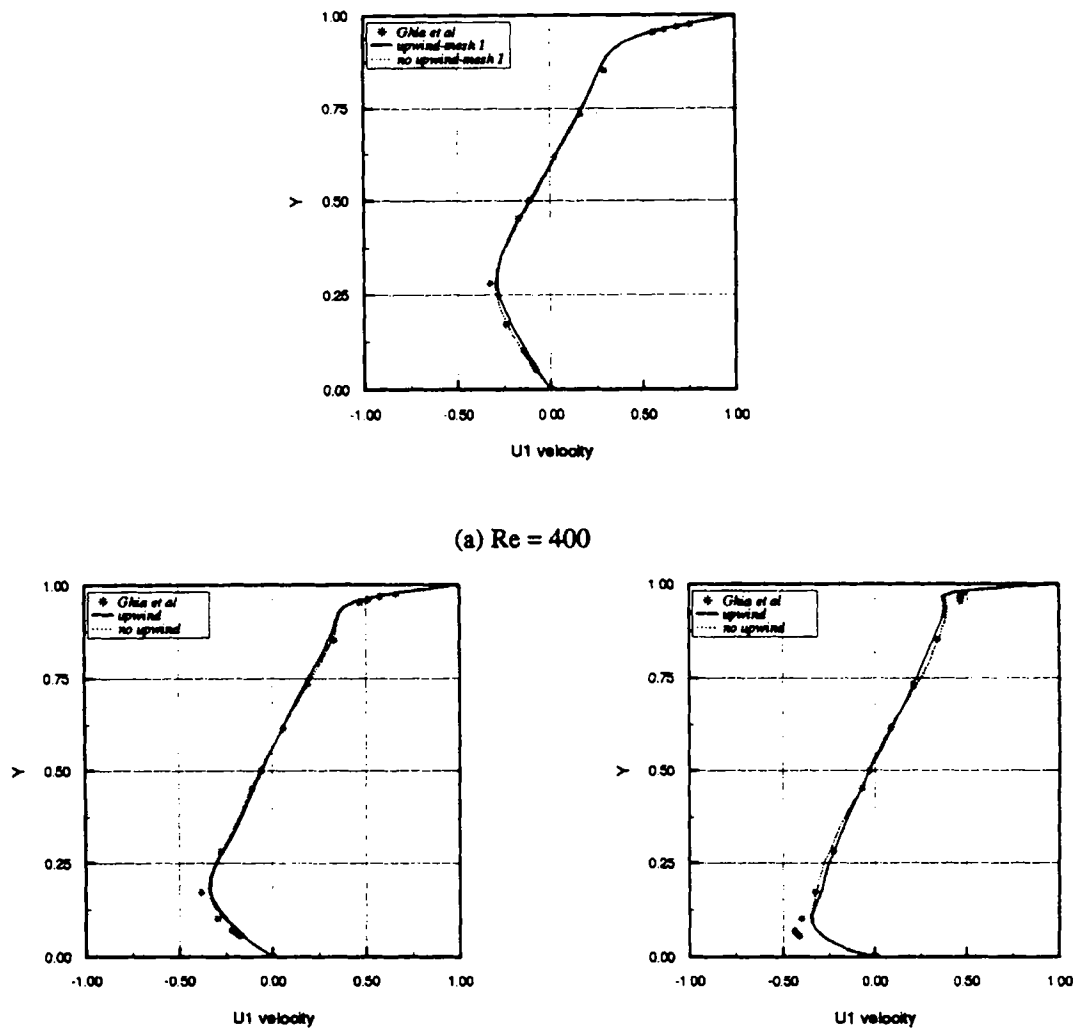

Figure 8. Comparison of U_1-velocity along mid-vertical plane with results of Ghia *et al.*[27] for various Reynolds numbers

number is taken as 3025. A very fine mesh is required near the wall boundaries owing to the large velocity gradients present there. Figure 11 shows the linear triangular element mesh used for this problem. It consists of 2714 nodes and 5212 elements. The nearest node from the wall is taken at a distance of $y^+ = 0{\cdot}7$, where

$$y^+ = \frac{y}{\nu}\sqrt{\left(\frac{\tau_0}{\rho}\right)}. \tag{45}$$

Here y is the normal distance from the nearest wall and τ_0 is the wall shear stress. The same boundary conditions as in Figure 1(a) are applied for velocities and pressure, except that a turbulent velocity profile is prescribed at the inlet. $\kappa = 0$ is prescribed on all the walls, while at the inlet a turbulent

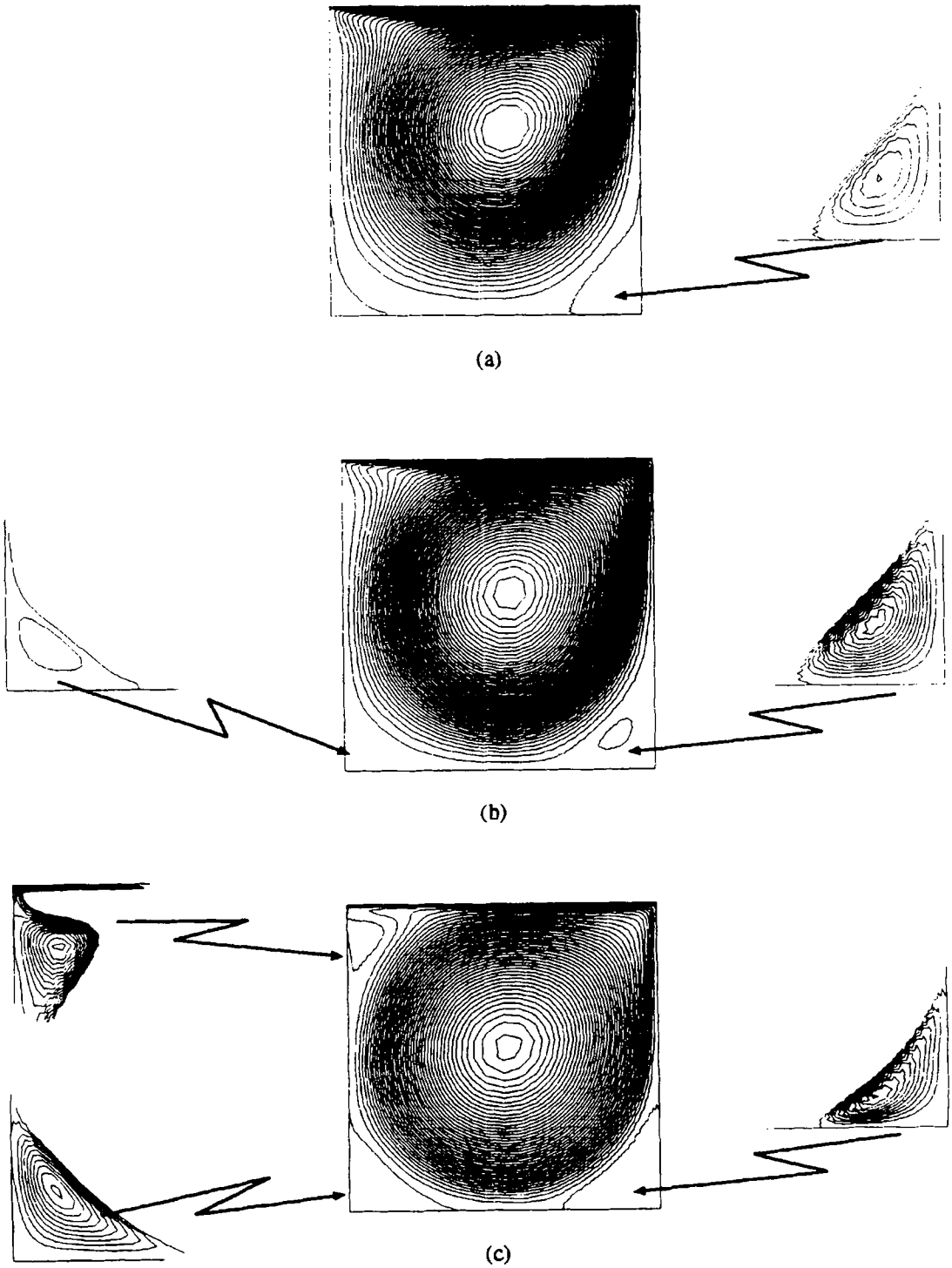

Figure 9. Streamlines for lid-driven cavity problem using present scheme: (a) $Re = 400$; (b) $Re = 1000$; (c) $Re = 5000$ (insets show streamlines in secondary circulation zones with smaller contour intervals)

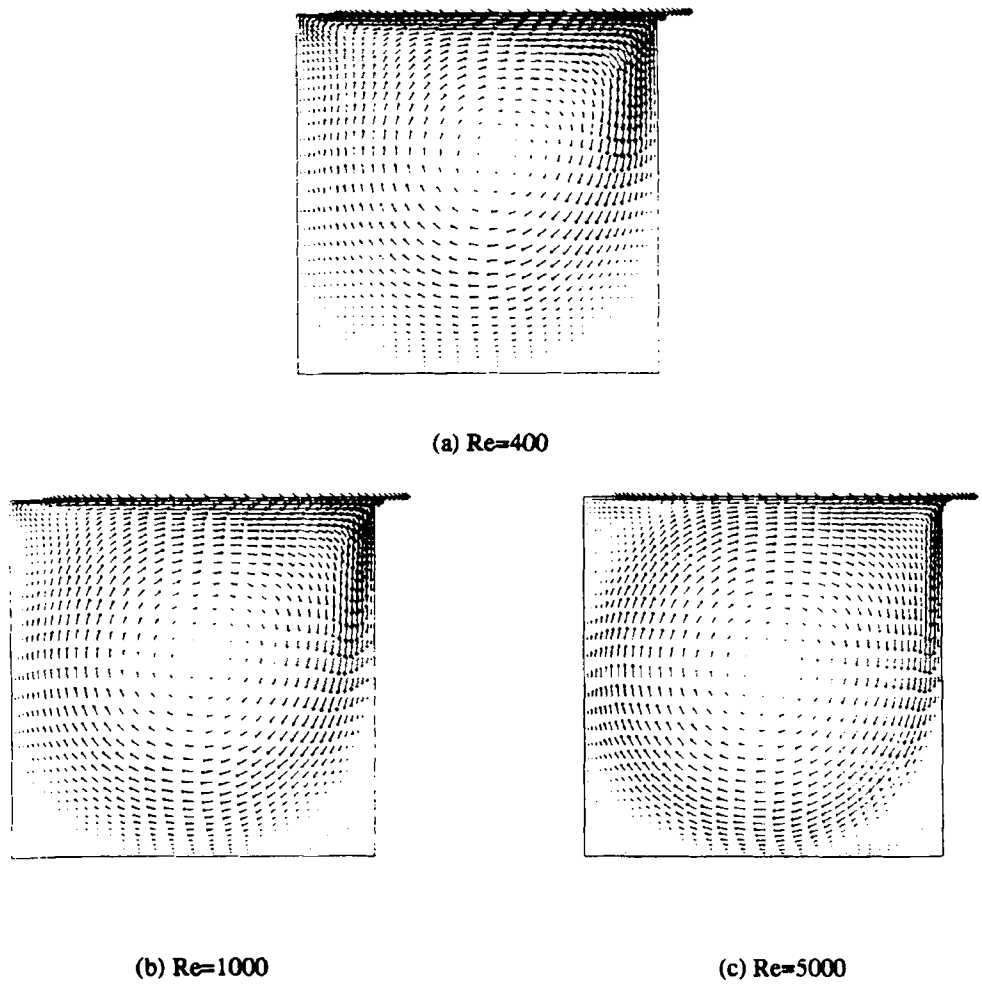

Figure 10. Velocity vectors for lid-driven cavity problem using present scheme

kinetic energy profile is prescribed. The velocity and turbulent kinetic energy profiles for the inlet are obtained from a one equation model analysis of turbulent flow through a channel of width same as at upstream of the step. Figure 12(a) shows the mesh for channel flow with $Re = 3025$. Freestream conditions are prescribed at the inlet for velocities and turbulent kinetic energy. The fully developed profiles for velocity and turbulent kinetic energy obtained at the outlet are shown in Figures 12(b) and 12(c) respectively. These profiles are used at the inlet for both one and two equation model analyses for the step. In addition, for the two equation model analysis an inlet ϵ-profile as obtained from the channel analysis is applied. On all the walls the condition $\partial\epsilon/\partial n = 0$ is applied. This is compatible with the damping functions used in the present analysis. It has been observed that for turbulent flows the present scheme does not result in an overdamping of flow quantities such as velocities and turbulent kinetic energy as was noted by some earlier investigators.[20,26] This is due to the formula used for evaluating Pe (see equation (44)). In the mean turbulent flow where there are higher velocities, the turbulent viscosity is also relatively high. This gives a smaller value of Pe, which in turn gives a smaller interior Δt. Thus very little damping is added in turbulent flow

Figure 11. Mesh (2714 nodes, 5212 elements) for turbulent flow past a backward facing step

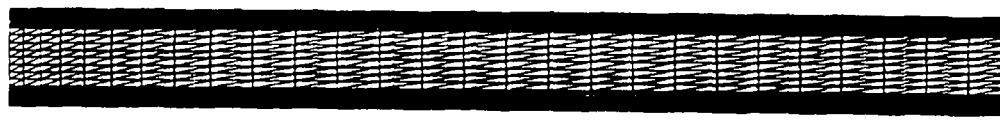

(a) Mesh, 1036 nodes, 1944 elements

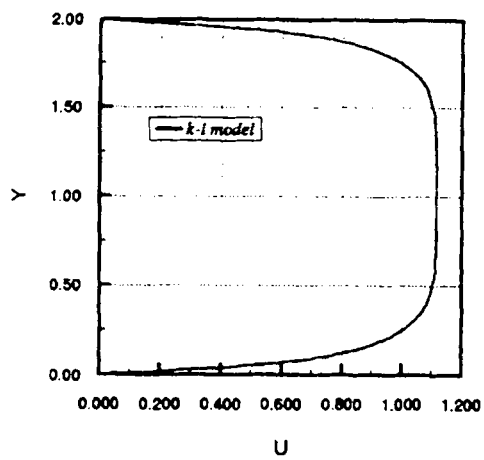

(b) Velocity profile at the exit

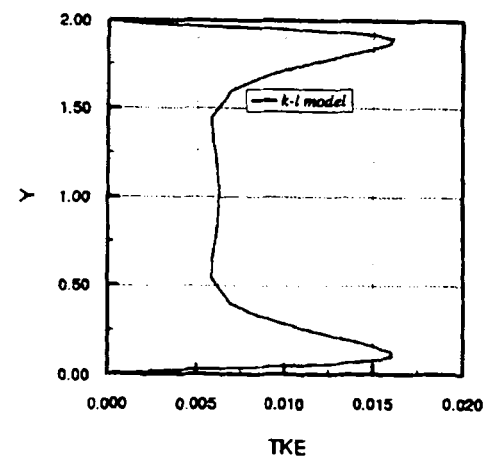

(c) Turbulent kinetic energy at the exit

Figure 12. Turbulent flow in a constant section channel, k–l model

situations. For the one equation model, Figures 13(a) and 13(b) show the velocity and turbulence intensity profiles respectively at various sections downstream of the step compared with the experimental profiles obtained by Denham *et al.*[31] Except for a small region in the circulation zone, in general there seems to be good agreement between the two. Figure 13(c) shows the streamline pattern for this case. Also shown is an enlarged view of the streamline pattern near the step. The reattachment length predicted by this model is $5{\cdot}6h$–$5{\cdot}7h$ as compared with $0{\cdot}6h$ by experiments. Here h is the step height. The corresponding predictions by Taylor *et al.*[26] and Atkins *et al.*[20] are $5{\cdot}6h$ and $5{\cdot}2h$ respectively. Figure 14 shows similar plots obtained from the present scheme by applying the two equation model of turbulence. The significant differences observed are in the recirculation zone, where the turbulent kinetic energy prediction of the one equation model is slightly better than

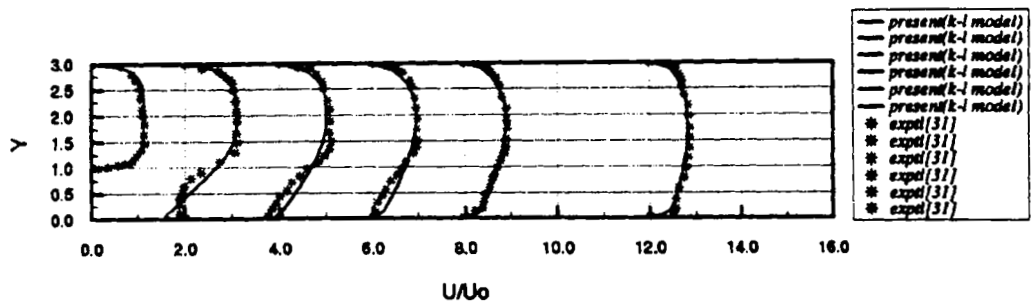

1 unit of U/U_o= 1 unit of X/h

(a) Velocity profiles downward of the step

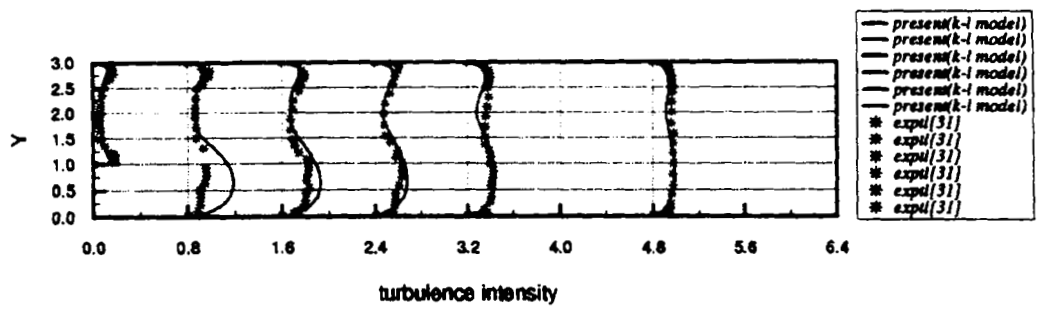

1 unit of T.I. = 2.5 units of X/h

(b) Turbulence intensity profiles downward of the step

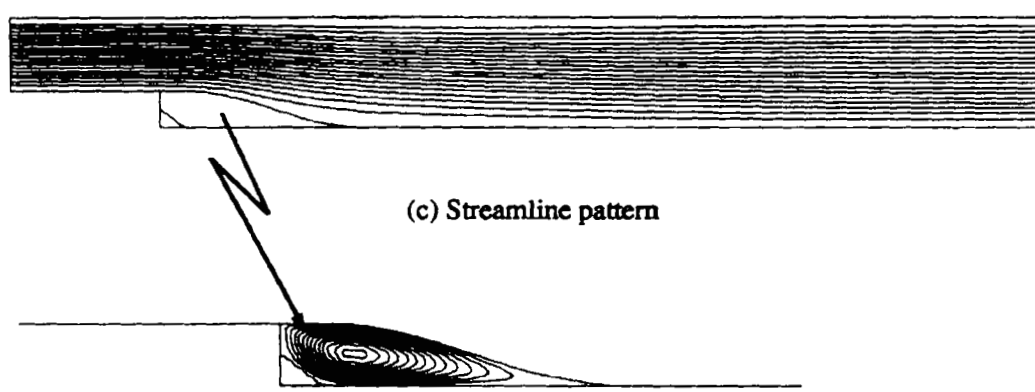

(c) Streamline pattern

Figure 13. Results for one equation model of turbulence for $Re = 3025$ using present scheme

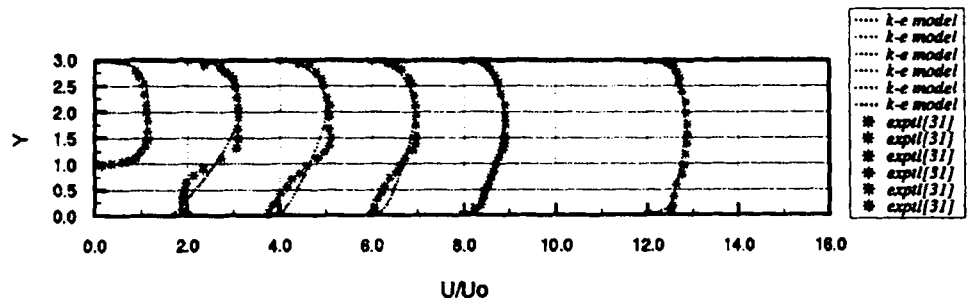

1 unit of U/U_o = 1 unit of X/h

(a) Velocity profiles downward of the step

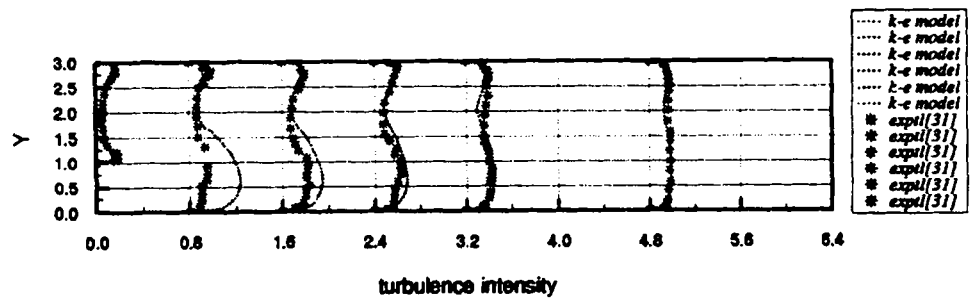

1 unit of T.I. = 2.5 units of X/h

(b) Turbulence intensity profiles downward of the step

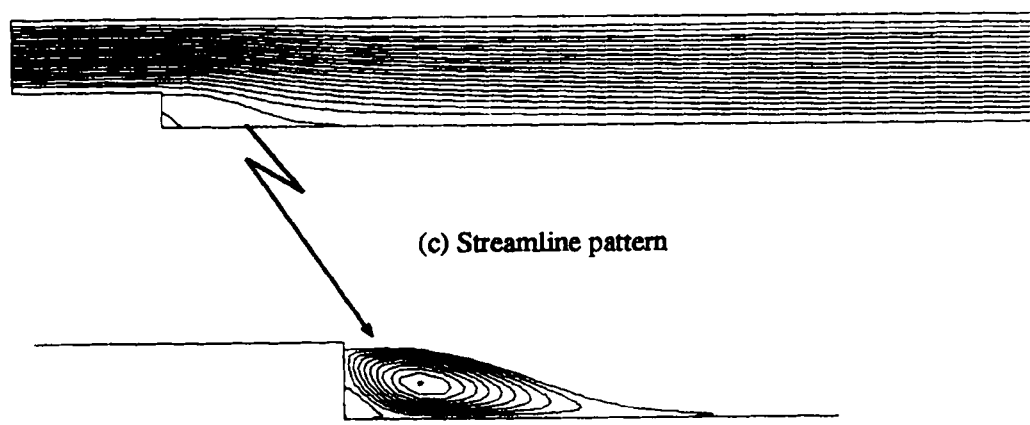

(c) Streamline pattern

Figure 14. Results for two equation model of turbulence for $Re = 3025$ using present scheme

that of the two-equation model. Also, the reattachment length for the two-equation model is $4{\cdot}7h$–$4{\cdot}8h$ as compared with $5{\cdot}6h$–$5{\cdot}7h$ for the one-equation model. The corresponding predictions by Taylor *et al.*[26] and Atkins *et al.*[20] are $4{\cdot}5h$ and $4{\cdot}2h$ respectively. Similar observations about the poorer performance of the two- equation model compared with the one-equation model for the backward-facing step problem were made by several investigators. Thus this section shows the applicability of the present scheme in making turbulent flow predictions.

7. CONCLUSIONS

The general fluid mechanics algorithm originally presented in Reference 19 has been applied in its semi-implicit form to laminar and turbulent flow situations. Satisfactory predictions are obtained both for laminar flow over a backward-facing step and for the lid-driven cavity problem. The scheme has also been extended for turbulent flow situations incorporating both one- and two-equation models. Satisfactory predictions of reattachment lengths were made with the present scheme. By using the modification for the Peclet number calculation, it is possible to avoid the overdamping effect of upwinding for turbulent flow problems.

REFERENCES

1. P. Hood and C. Taylor, 'Navier–Stokes equations using mixed interpolation', in J. T. Oden *et al.* (eds), *Finite Element Methods in Flow Problems*, UAH Press, Huntsville, AL, 1974, pp. 121–132.
2. O. C. Zienkiewicz and R. L. Taylor, *The Finite Element Method*, 4th edn, McGraw-Hill, New York, 1989.
3. T. J. R. Hughes, L. P. Franca and M. Balastra, 'A new finite element formulation for computational fluid dynamics: V. Circumventing the Babŭska–Brezzi condition: a stable Petrov–Galerkin formulation of the Stokes problems accommodating equal-order interpolations', *Comput. Methods Appl. Mech. Eng.*, **59**, 85–99 (1986).
4. R. L. Sani, P. M. Gresho, R. L. Lee and D. F. Griffiths, 'The cause and cure(?) of the spurious pressure generated by certain FEM solutions of the incompressible Navier–Stokes equations: Part I', *Int. j. numer. methods fluids*, **1**, 17–43 (1981).
5. R. L. Sani, P. M. Gresho, R. L. Lee, D. F. Griffiths and M. Engleman, 'The cause and cure(!) of the spurious pressure generated by certain FEM solutions of the incompressible Navier–Stokes equations: Part II', *Int. j. numer. methods fluids*, **1**, 171–204 (1981).
6. A. J. Chorin, 'Numerical solution of the Navier–Stokes equations', *Math. Comput.*, **23**, 341–354 (1968).
7. G. E. Schneider, G. D. Raithby and M. M. Yovanovich, 'Finite element analysis of incompressible fluid flow incorporating equal order pressure and velocity interpolation', in C. Taylor, K. Morgan and C. A. Brebbia (eds), *Numerical Methods in Laminar and Turbulent Flow*, Pentech, 1978.
8. M. Kawahara and K. Ohmiya, 'Finite element analysis of density flow using the velocity correction method', *Int. j. numer. methods fluids*, **5**, 308–323 (1985).
9. B. Ramaswamy, 'Finite element solution for advection and natural convection flows', *Comput. Fluids*, **16**, 349–388 (1988).
10. O. C. Zienkiewicz and J. Wu, 'A general explicit or semi-explicit algorithm for compressible or incompressible flows', *Int. j. numer. methods eng.*, **35**, 457–459 (1992).
11. O. C. Zienkiewicz and J. Wu, 'Incompressibility without tears—how to avoid the restrictions on mixed formulation', *Int. j. numer. methods eng.*, **32**, 1189–1203 (1991).
12. P. Gresho and R. L. Lee, 'Don't suppress wiggles—they are telling you something', *Comput. Fluids*, **9**, 223–253 (1981).
13. I. Christie, D. F. Griffiths, A. R. Mitchell and O. C. Zienkiewicz, 'Finite element methods for second-order differential equations with significant first-order derivatives', *Int. j. numer. methods eng.*, **10**, 1389–1396 (1976).
14. J. C. Heinrich, P. S. Huyakorn, A. R. Mitchell and O. C. Zienkiewicz, 'An upwind finite element scheme for two dimensional convective transport equations', *Int. j. numer. methods eng.*, **11**, 131–144 (1977).
15. T. J. R. Hughes and A. N. Brooks, 'A multi-dimensional upwind scheme with no cross wind diffusion', in T. J. R. Hughes (ed.), *Finite Elements for Convection Dominated Flows*, AMD Vol. 34, ASME, New York, 1979.
16. D. N. Kelly, S. Nakazawa, O. C. Zienkiewicz and J. C. Heinrich, 'A note on anisotropic balancing dissipation in finite element method approximation to convection diffusion problems', *Int. j. numer. methods eng.*, **15**, 1705–1711 (1980).
17. C. Johnson, U. Navert and J. Pitkaranta, 'Finite element method for linear hyperbolic problems', *Comput. Methods Appl. Mech. Eng.*, **45**, 288–312 (1984).
18. R. Lohner, K. Morgan and O. C. Zienkiewicz, 'The solution of non- linear hyperbolic equation systems by the finite element method', *Int. j. numer. methods fluids*, **4**, 1043–1063 (1984).
19. O. C. Zienkiewicz and R. Codina, 'A general algorithm for compressible and incompressible flow, Part I: The split, characteristic-based scheme', *Int. j. numer. methods fluids*, **20**, 869–885 (1995).
20. D. J. Atkins, S. J. Maskell and M. A. Patrick, 'Numerical prediction on separated flows', *Int. j. numer. methods eng.*, **15**, 129– 144 (1980).

21. W. Rodi, *Turbulence Models and Their Applications in Hydraulics— A State of the Art Review*, IAHR.
22. M. Wolfstein, 'Some solutions of plane turbulent impinging jets', *ASME J. Basic Eng.*, **92**, 915–922 (1970).
23. C. K. G. Lam and K. Bermhorst, 'A modified form of κ–ϵ model for predicting wall turbulence', *J. Fluids Eng.*, **103**, 456–460 (1981).
24. R. Codina, M. Vázquez and O. C. Zienkiewicz, 'A fractional step method for compressible flows: boundary conditions and incompressible limit', *Proc. Int. Conf. on Finite Elements in Fluids—New Trends and Applications*, Venice, October 1995, pp. 409–418.
25. M. K. Denham and M. A. Patrick, 'Laminar flow over a downstream- facing step in a two-dimensional flow channel', *Trans. Inst. Chem. Eng.*, **52**(4), 361–367 (1974).
26. C. Taylor, C. E. Thomas and K. Morgan, 'Analysis of turbulent flow with separation using the finite element method', in C. Taylor and K. Morgan (eds), *Recent Advances in Numerical Methods in Fluids*, Vol. 2, *Computational Techniques in Transient and Turbulent Flow*, Pineridge, Swansea, 1981, pp. 283–325.
27. U. Ghia, K. N. Ghia and C. T. Shin, 'High-Re solutions for incompressible flow using the Navier–Stokes equations and a multi-grid', *J. Comput. Phys.*, **48**, 387–411 (1982).
28. J. L. Sohn, 'Evaluation of FIDAP on some classical laminar and turbulent benchmarks', *Int. j. numer. methods fluids*, **8**, 1469–1490 (1988).
29. L. P. Hackman, G. D. Raithby and A. B. Strong, 'Numerical predictions of flows over backward facing steps', *Int. j. numer. methods fluids*, **4**, 711–724 (1984).
30. A. Autret, M. Grandotto and I. Dekeyser, 'Finite element computation of a turbulent flow over a two-dimensional backward-facing step', *Int. j. numer. methods fluids*, **7**, 89–102 (1987).
31. M. K. Denham, P. Briard and M. A. Patrick, 'A directionally sensitive laser anemometer for velocity measurements in highly turbulent flow', *J. Phys. E: Sci. Instrum.*, **8**, 681–683 (1975).
32. O. C. Zienkiewicz, K. Morgan, B. V. K. Satya Sai, R. Codina and M. Vázquez, 'A general algorithm for compressible and incompressible flow, Part II: Tests on the explicit form', *Int. j. numer. methods fluids*, **20**, 887–913 (1995).